ANALYSIS OF PLASMA BEHAVIOR FOR A MAGNETIC THRUST CHAMBER OF LASER FUSION ROCKET BY USING 3D HYBRID CODE

Hideyuki Uchimura, Takanobu Muranaka and Hideki Nakashima

Department of Advanced Energy Engineering Science, Kyushu University,
6-1 Kasuga-Kouen, Fukuoka 816-8580, JAPAN

Abstract

A magnetic thrust chamber concept in a laser fusion rocket is suitable for controlling the plasma flow, and it has an advantage in that thermalization with wall structures in a thrust chamber can be avoided. A three-dimensional (3D) hybrid particle-in-cell (PIC) code has been developed to analyze the plasma behaviors in the magnetic thrust chamber. The magnetic field structure adopted is a variant from a dipole type field, since with decreasing coil radius the field structure reproduces that of a dipole type field. Plasma behaviors in a dipole field are also examined and comparison is made among the experimental data, MHD analysis and the results from the 3D hybrid code. So far, an overall good agreement among these results was found.

1.Introduction

Fusion reaction can release a large amount of energy, and it could easily produce high temperature and density plasma. The resulting plasma flow could be controlled by a properly designed applied magnetic field geometry, i.e., a magnetic thrust chamber. In a laser fusion rocket, the chamber is composed of a solenoidal superconducting coil. The fusion reaction occurs by irradiation of a laser onto a fuel pellet, and the the plasma generated expands isotropically at an early stage; it is then deflected by the magnetic field and finally exhausted from the chamber. The chamber has an advantage in that thermalization with wall structures in a thrust chamber can be avoided. Thus, the laser fusion rocket could realize a very high exhaust velocity of plasma as compared with existing systems. This fact makes the laser fusion rocket a promising candidate for an interplanetary transport system.

Recently, an analysis has been made of plasma behaviors in a magnetic field configuration modeling a magnetic thrust chamber for a laser fusion rocket[1] and the thrust efficiency was estimated by using a 3D hybrid code.

The magnetic field structure adopted is a variant from a dipole type field, since with decreasing coil radius the field structure reproduces that of a dipole type field.

On the other hand, for a dipole field configuration, Nikitin & Ponomarenko[2] have analyzed the dynamics of 3D plasma expansion in the framework of the ideal magnetohydrodynamics (MHD) approximation. By comparing the results from the MHD calculation with the experimental data, they have found an important parameter (κ) characterizing the interaction of expanding plasma cloud with the dipole field. Furthermore, they have applied the same method to estimation of the thrust efficiency in the magnetic thrust chamber and compared their results to those from the 3D hybrid code. They have found a good agreement between them[3].

The plan of the paper is as follows: Section 2 presents an analysis of the plasma behavior in a magnetic thrust chamber of laser fusion rocket. An analysis of the plasma behavior in a dipole field is presented in Sec. 3. We compare those results from the 3D hybrid code with the experimental data and the MHD analysis there. The conclusions are given in Sec. 4.

2.Analysis of plasma behavior in a magnetic thrust chamber of laser fusion rocket

The calculational model adopted here is illustrated in Fig. 1, which is based on a configuration of a laser fusion rocket proposed by Hyde[4]. The calculational parameters used in the simulation are shown in Table 1.

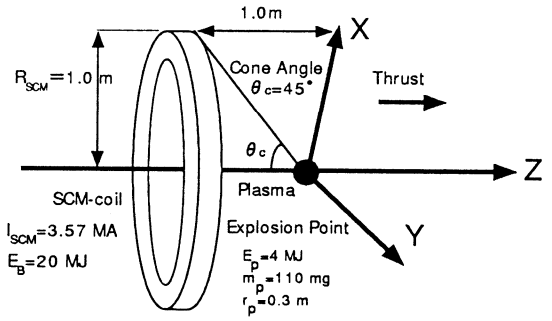

Fig. 1 Schematic of the calculational model.

We proposed to use ignition facilities such as the National Ignition Facilities (NIF) to examine the feasibility of the magnetic thrust chamber concept[5]. A schematic layout of the setup is shown in Fig. 2. Thus, the configuration studied here takes

utilization of the facility into account; i.e., an NIF experimental configuration is treated here.

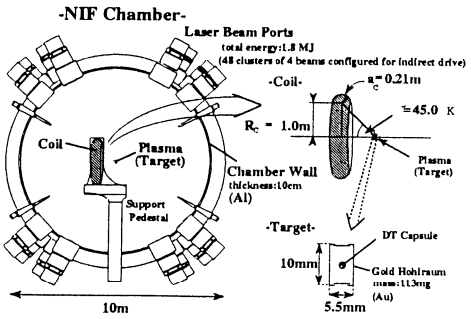

Fig. 2 Schematic of layout of the experimental setup in the NIF chamber.

Table 1 Calculational parameters

Plasma energy (MJ)	4
Plasma mass (mg)	110
Plasma radius (m)	0.3
Atomic mass (AMU)	197
Atomic number	79
Effective charge (C)	16.81
Electron temperature (eV)	0
SCM radius (m)	1.0
Initial magnetic field strength at the coil axis (T)	2.12
Cone angle (deg)	45

The fusion target, the indirect cyrotarget, has a small deutrium-tritium fuel/CH ablator capsule inside a gold hohlraum, the target mass (113mg) being dominated by gold. The target is irradiated by lasers with an energy of 1.8MJ.

A value of 20MJ is adopted here for a representative fusion yield, 20 % of which is carried by plasma. Its ionic charge is calculated from the simulation results for the NIF indirect drive target in Ref. [6] by using the Thomas-Fermi model. A value of 16.81 is obtained for the ionic charge of gold at a temperature of 100eV and a density of 1.0g/cm^3. This charge number is given to all the ions simulated.

The initial plasma is assumed to have a radius r_p of 0.3m and is entirely composed of gold the mass m_p of which is 110mg. The initial kinetic energy of plasma debris E_p is assumed as 4MJ. The initial density and velocity distributions are assumed as uniform. An angle θ_c (cone angle) subtended from the initial plasma position at the z axis to the solenoidal coil is taken to be 45 deg.

To calculate the plasma behavior under the magnetic field, we have developed a 3D hybrid PIC code based on the model given in Ref. [7]. The basic equations in the code are as follows: The magnetic field is generated by a solenoidal magnet coil, which is, for convenience, approximated as a simple current loop. The analytical solution for a vector potential produced by the loop is given in cylindrical coordinate as

$$A_\theta(r,\theta,z) = \frac{\mu_0 I\sqrt{R}}{\pi k\sqrt{r}} \times \left\{ \left(1 - \frac{1}{2}k^2 K(k^2)\right) - E(k^2) \right\} \quad (1)$$

where the argument of the elliptic integrals E and K is given by

$$k^2 = \frac{4rR}{(r+R)^2 + (z-X)^2} \quad (2)$$

where again X express the coil position and r,θ and z are taken as shown in Fig. 3.

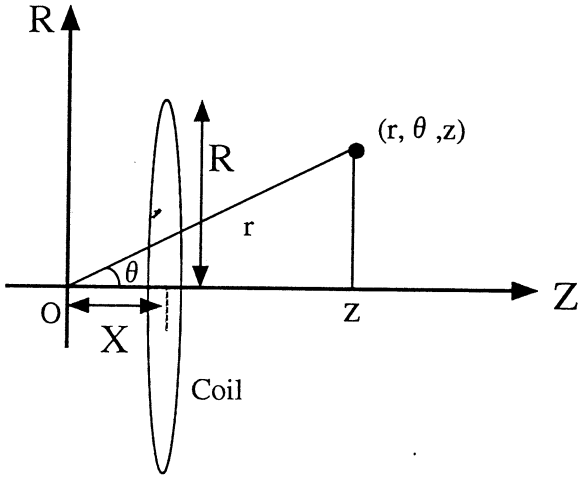

Fig. 3 Coordinate system for vector potential.

It is noted that A_θ is the only component that exists because the coil current is entirely in the θ direction. Then the magnetic flux $\boldsymbol{B}$ is obtained from the relation

$$\boldsymbol{B} = \nabla \times \boldsymbol{A} \quad (3)$$

Kinetic equations of an individual ion with mass m_i, charge Ze, velocity $\boldsymbol{v}_i$ and particle position $\boldsymbol{x}_i$ are given by

$$\frac{d\boldsymbol{v}_i}{dt} = \frac{Ze}{m_i}(\boldsymbol{E} + \boldsymbol{v}_i \times \boldsymbol{B}) \quad (4)$$

and

$$\frac{d\boldsymbol{x}_i}{dt} = \boldsymbol{v}_i \quad , \quad (5)$$

where e is the elementary electric charge, Z atomic number, $\boldsymbol{E}$ electric field and $\boldsymbol{B}$ magnetic field.

The kinetic equation of the inertialess electron fluid is given by

$$\begin{aligned} n_e m_e \frac{d\boldsymbol{v}_e}{dt} &= -en_e(\boldsymbol{E} + \boldsymbol{v}_e \times \boldsymbol{B}) - \nabla P_e \\ &= 0 \quad , \end{aligned} \quad (6)$$

where m_e is the electron mass, v_e the electron velosity, and P_e the electron pressure given by

$$P_e = n_e T_e, \tag{7}$$

where T_e is the electron temperature. Ampere's law is given by

$$\nabla \times \boldsymbol{B} = \mu_0(\boldsymbol{J}_e + \boldsymbol{J}_i) \tag{8}$$

where $\boldsymbol{J}_i$ and $\boldsymbol{J}_e$ are the ion and electron current densities, respectively, and μ_0 is the vacuum permeability, the transverse displacement current being neglected.

Eliminating v_e in Eq.(6) by using Eq.(8) and the definition of the electron current density

$$\boldsymbol{J}_e = -e n_e \boldsymbol{v}_e, \tag{9}$$

we obtain the following equation to solve the electric field:

$$\boldsymbol{E} = \frac{1}{n_i e}\left(\frac{1}{\mu_0 Z}(\nabla \times \boldsymbol{B}) \times \boldsymbol{B} - \frac{1}{Z}\boldsymbol{J}_i \times \boldsymbol{B} - T_e \nabla n_i\right), \tag{10}$$

where Eq.(7) is used for P_e, assuming that the T_e is uniform. We assume quasi-neutrality and set the ion charge density equal to the electron charge density i.e., $Z n_i = n_e$. The ion density n_i and the current density $\boldsymbol{J}_i$ are calculated by the PIC method from the particle position $\boldsymbol{x}_i$ and the velocity $\boldsymbol{v}_i$.

The magnetic field is advanced by Faraday's law:

$$\frac{\partial \boldsymbol{B}}{\partial t} = -\nabla \times \boldsymbol{E} \tag{11}$$

Cartesian coordinates are adopted here. The boundary condition adopted here for the field quantities is that the spatial differences of the normal components are set to be zero.

The plasma behaviors calculated by the three dimensional hybrid PIC code are shown in Fig. 4, where we plot plasma positions projected onto the xz plane at t=0, 4 and 8 μsec. The plasma initially expands isotropically, and then it is reflected back from compressed magnetic field, resulting in thrust.

The thrust efficiency η in terms of momentum is calculated as follows:

$$\eta = \frac{\sum m_i v_z}{\sum m_i |v_0|}, \tag{12}$$

where v_z is the z-component of ion velocity, and $|v_0|$ the absolute value of initial velocity. The sum (Σ) is carried over all plasma particles. The results are shown in Fig. 5. as a function of time. The value of η increases rapidly between 1 and 6 μsec, and then its value saturates around 65% at $\sim$ 8μsec.

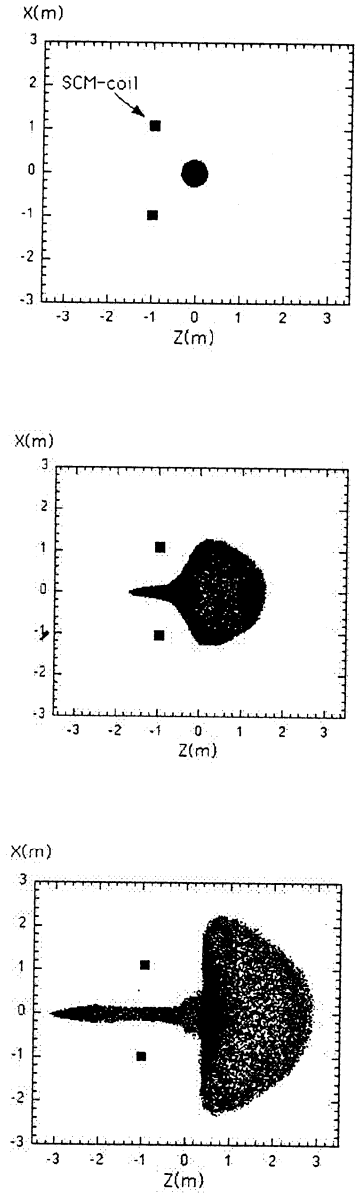

Fig. 4 Plasma positions projected onto the xz plane at t=0, 4 and 8 μsec.

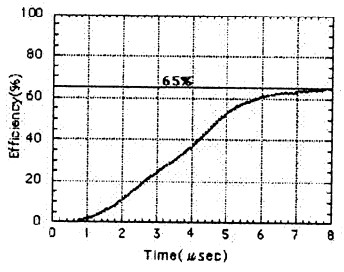

Fig. 5 Time evolution of the thrust efficiency.

3.Analysis of exploding plasma behavior in a dipole magnetic field

3.1 Experimental facility and numerical model

For the comparative analysis, we will use the data of experiment of [2] where quasi-spherical clouds of laser plasma were produced by means of the bilateral symmetric action of a CO_2- laser pulse on a small Nylon $(C_6H_{11}ON)_n$ target placed in a vacuum chamber near a current coil with magnetic moment amplitude $|m|$=11 MG·cm^3. Figure 6 shows a schematic of the experimental facility.

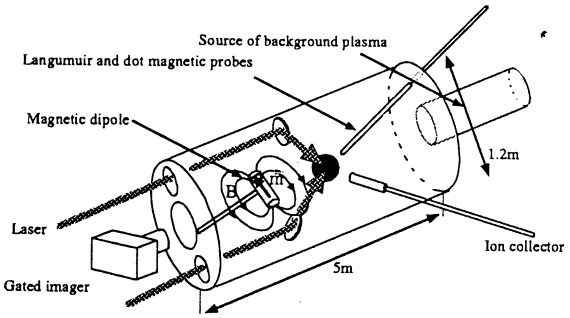

Fig. 6 Schematic of experimental facility

The experimental parameters are given in Table 2. The explosion is assumed to take place in the equatorial plane at radius R_e = 21.6 cm at a point with field B = 0.11 T. The kinetic energy of the plasma cloud E_0 is 13 J.

Table 2 Experimental parameters

Initial magnetic field at R = Re (T)	0.11
Dipole magnetic moment $\|m\|$ (MG · cm^3)	11
Distance of its center from the target Re (cm)	21.6
Initial kinetic energy E_0 (J)	13
Ion charge state Z (H^+ 50%, C^{4+} 50%)	2.5
Plasma mass state (AMU)	6.5

A parameter (interaction parameter) κ is defined as

$$\kappa = \frac{E_0}{E_M} = \frac{3E_0R_e^3}{|m|^2}, \qquad (13)$$

where E_M is the field energy integral of the dipole within a spherical radius R_e ($E_M = |m|^2/3R_e^3$). It characterizes the interaction between the expanding plasma and the dipole field[2].

The parameter is estimated from Table 2 to be 0.036 in this experiment and a substantial plasma deceleration will occur in all directions from the explosion location ("quasi-capture" mode).

The calculational model adopted here is illustrated in Fig. 7, which is based on the experimental configuration given in Ref. [2].

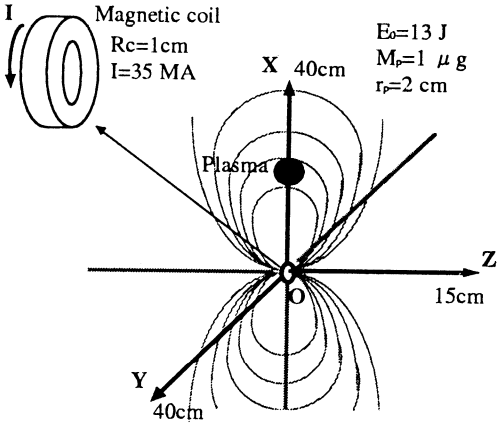

Fig. 7 Schematic of the calculational model

The initial plasma is assumed to have a radius of 2 cm with a mass of 1 μg. The dimensions (X ×Y × Z) of the calculational region are 80 cm × 80 cm × 30 cm, and the calculational geometry is cylindrical along z axis. The mesh size adopted is (1cm)^3 . The number of the simulated particle is 100,000. The coil to produce the dipole field is assumed to have a radius of 1cm with a current density of 35MA.

3.2 Comparison with experimental data and MHD analysis

The plasma behaviors calculated by the 3D hybrid code are shown in Figs. 8(a) and 8(b) where particle positions are projected onto the xz and xy planes at t=0.1, 0.37, 0.64 and 0.91 μsec, respectively. Here, the simulation starts from t = 0.1 μsec to take account of the time elapsed for the plasma expansion to 2 cm. Plasma shape is spherical at the initial stage, and then its shape changes to follow the dipole magnetic field. It is found that the plasma particles in the calculation are captured by the dipole magnetic field in the xz plane. On the other hand, as shown in Fig. 8(b) the plasma cloud is not symmetric in the xy plane after 0.37 μsec. Figures 9(a) and 9(b) show the velocity distribution projected onto the xz and xy planes at t=0.64 μsec, respectively. From these figures, this asymmetrical pattern is thought to be caused by the diamagnetic motion plus the force from the magnetic field.

Figure 10(a) shows the front of the plasma cloud, represented by dashes, obtained with the aid of a sensitive image-converter tube at time t = 0.7 μsec after the laser pulse. Also shown here for comparison are the results from the MHD calculations as the shaded area. Figure 10(b) shows a plot of particle positions obtained from the 3D hybrid calculation.

From these results, we found an overall good agreement among these results. A densification of the particles is observed in the plot of simulation results (Fig. 10(b)), due to the reflection of particles from the inner magnetic field.

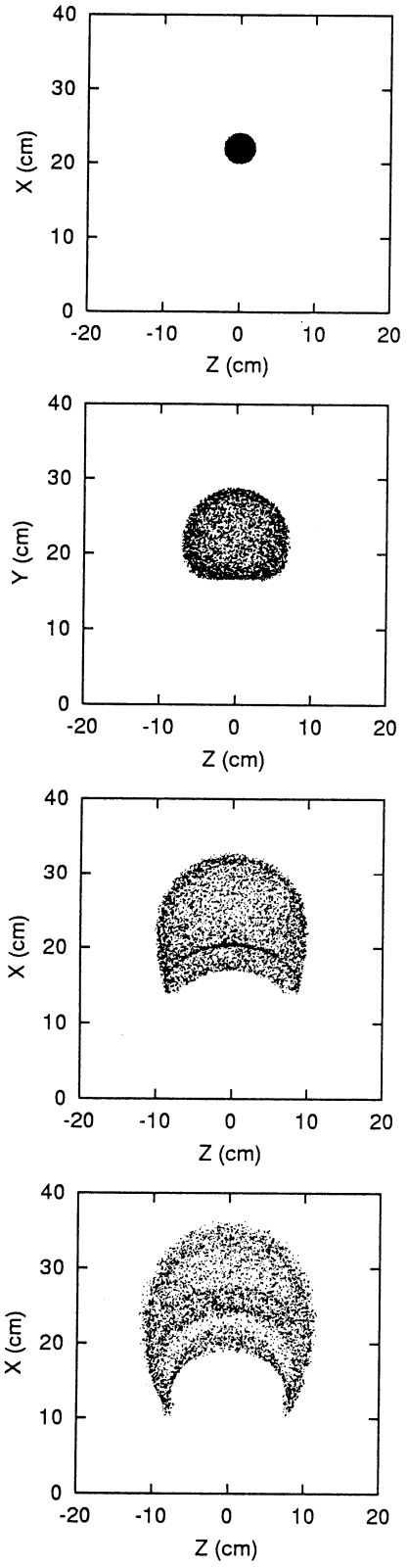

Fig. 8(a) Simulation results (κ=0.036) -particle positions projected onto the xz plane at t=0.1, 0.37, 0.64 and 0.91 μsec-

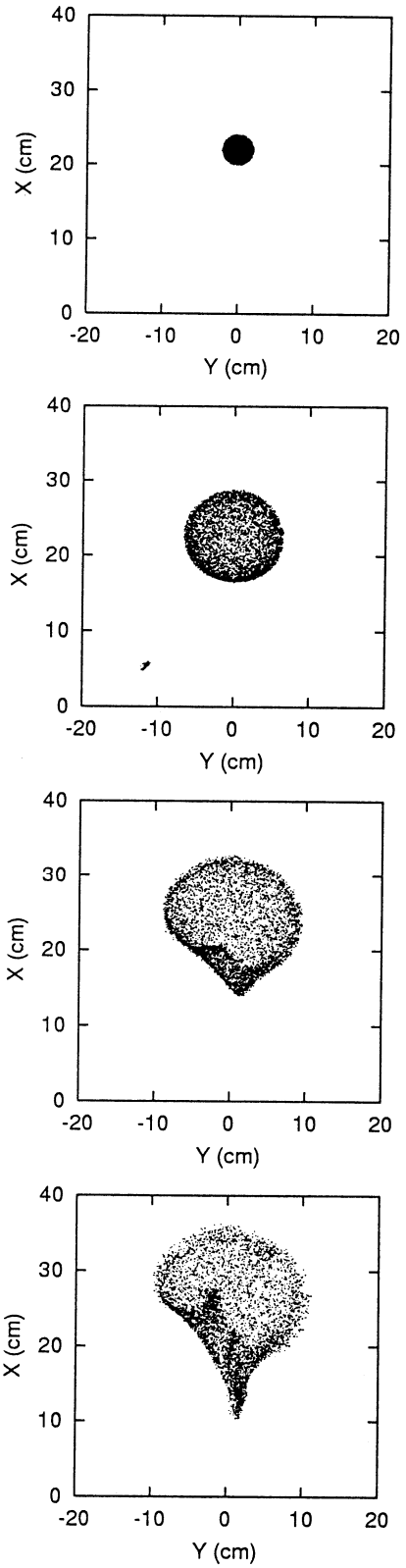

Fig. 8(b) Simulation results (κ=0.036) -particle positions projected onto the xy plane at t=0.1, 0.37, 0.64 and 0.91 μsec-

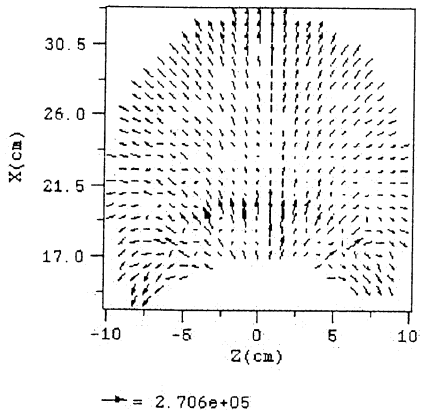

Fig. 9(a) Velocity distribution projected onto the xz plane at t=0.64 μsec. (κ =0.036)

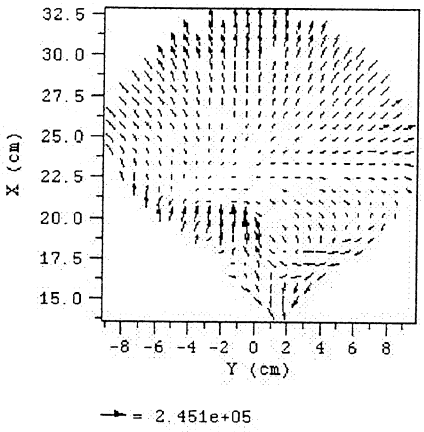

Fig. 9(b) Velocity distribution projected onto the xy plane at t=0.64 μsec. (κ =0.036)

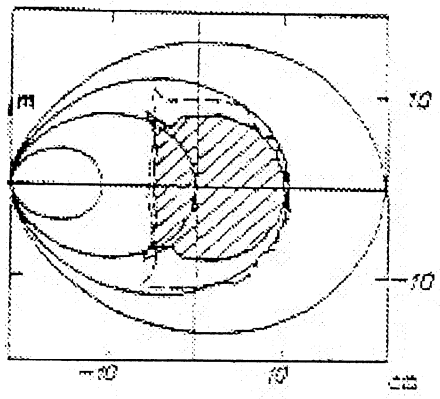

Fig. 10(a) Experimental data (dashed line) and MHD calculational results (shaded area) (κ = 0.036) -plasma cloud at time t=0.7 μsec after laser pulse-

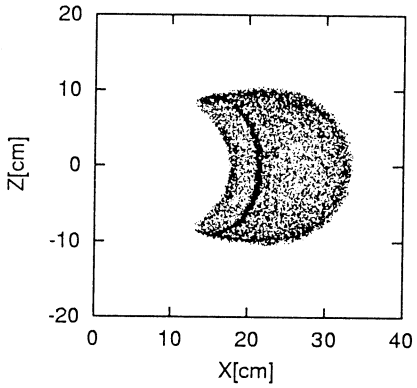

Fig. 10(b) Simulation results (κ=0.036) -particle positions projected onto the xz plane at t=0.7 μsec-

Figure 11(a) shows a picture taken at time = 1.73 μ sec after the laser pulse for the case of κ = 0.02 with the initial plasma energy of 8 J. Figure 11(b) shows the simulation result at time = 1.2 μsec after the laser pulse. We found from these results that still the plasma particles were captured by the dipole magnetic field. We will continue the simulation to obtain the results at t = 1.7 μsec.

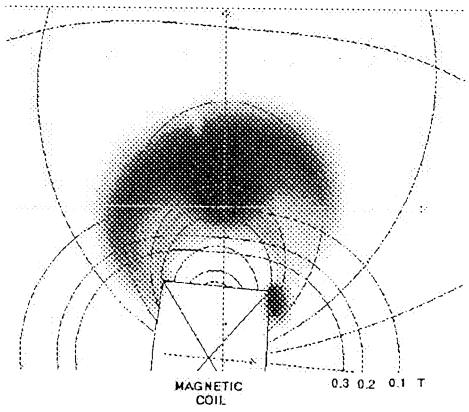

Fig. 11(a) Experimental data (κ = 0.02) -plasma cloud at time t=1.7 μsec after laser pulse-

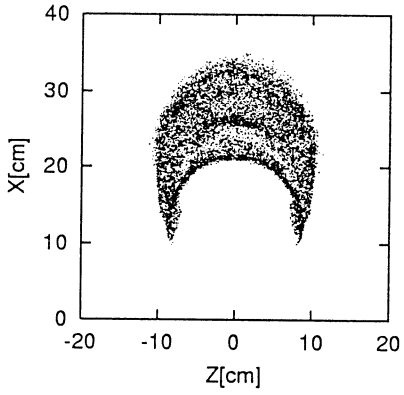

Fig. 11(b) Simulation results (κ=0.02) -particle positions projected in the xz plane at t=1.2 μsec-

The "rupture" regime was studied by increasing the initial plasma energy and then the interaction parameter κ. We tried to simulate the case of κ = 0.36 with the initial plasma energy of 130 J. The values are one order of magnitude larger than those in the previous "capture" mode. (Note that the critical value for κ between the two modes is 0.1)

Figure 12 shows the simulation result of particle positions projected onto the xz plane at time = 0.3 μsec after the laser pulse. Plasma particles are found to expand more rapidly at the early stage as compared with those in "capture mode"(Fig. 7(a)). At t=0.32 μsec, the plasma particles are found to run away from the calculational region.

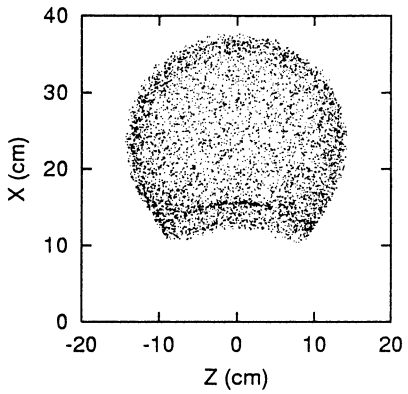

Fig. 12 Simulation results (κ=0.36)
-particle positions projected in the xz plane
at t=0.3 μsec-

4.Conclusion

First, an analysis of plasma behabiors in a magnetic thrust chamber of laser fusion rocket was made by using a 3D hybride code. We found that the thrust efficiency in terms of momentum is found to be 65 % for the case where the cone angle θ_c = 45 deg.

Next, an analysis was made of plasma behaviors in a dipole field by using a 3D hybrid code and comparison was made among the experimental data, MHD analysis and the results from the 3D hybrid code. So far, an overall good agreement among these results was found. Since the magnetic field structure adopted in a chamber of a laser fusion rocket is a variant from a dipole type field, these results will be useful in designing an optimal configuration of the magnetic thrust chamber.

References

[1] Y. Nagamine, H.Nakashima, Fusion Technology, **35**, 62(1999).
[2] S. A. Nikitin, A. G. Ponomarenko, J. Appl. Mech. Techn. Phys., **34**, 745(1993)
[3] S. A. Nikitin, A. G. Ponomarenko, Proc. ICENES 98, 299(1998).
[4] R. A. Hyde, UCRL-88857, Lawrence Berkley Laboratory (1983).
[5] H.Nakashima, et al. Fusion Eng. Des. , **44**, 359 (1999).
[6] R. P. Peterson et al., UWFDM-1008, University of Wisconsin, Madison (1996); see also R. P. Paterson et al., *Fusion Tecnol.*, **30**,431 (1996).
[7] D. S. Harned, J. Comput. Phys. , **47**, 452 (1982).